CHEMISTRY OF MATERIALS

pubs.acs.org/cm

Article

Revealing the Correlation between the Solvation Structures and the Transport Properties of Water-in-Salt Electrolytes

Xinyi Liu,[#] Shao-Chun Lee,[#] Soenke Seifert, Lilin He, Changwoo Do, Randall E. Winans, Gihan Kwon, Y Z,* and Tao Li*

Cite This: *Chem. Mater.* 2023, 35, 2088−2094

Read Online

ACCESS | Metrics & More | Article Recommendations | Supporting Information

ABSTRACT: Water-in-salt (WIS) electrolytes containing 21 m lithium bis(trifluoromethane sulfonyl)imide (LiTFSI) have been considered as a safe and environment-friendly alternative to common organic electrolytes used in lithium-ion batteries. However, the relation between the solvation structures and transport properties of these materials remains elusive. Herein, we performed small-angle X-ray scattering (SAXS), small-angle neutron scattering (SANS), and X-ray pair distribution function (PDF) measurements of LiTFSI aqueous solutions at a wide range of concentrations. Combined with molecular dynamics simulations, the detailed solvation structures from long to short length scale were resolved. We found that the $TFSI^-$ solvation structures consist of $TFSI^-$ solvated structures and $TFSI^-$ networks; the former corresponds to solvent separated ion pairs, while the latter corresponds to contact ion pairs and cation−anion aggregates. In addition, we found that the relaxation time in the q range associated with the anion network structure exhibits the same concentration dependence as the viscosity. By combining the results from the experiments and simulations, this study revealed a correlation between the solvation structures of LiTFSI and the transport properties of the solutions, which is critical to understand the relation between the transport properties and the dynamics of the ions for imide-based lithium-ion salt aqueous electrolytes.

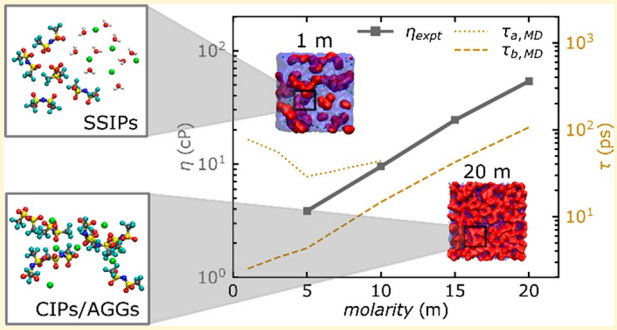

INTRODUCTION

The new aqueous "water-in-salt" (WIS) electrolytes containing 21 m (mol/kg) LiTFSI have attracted significant attention from the energy storage community because of their potential for application in supercapacitor and battery technologies.[1] WIS electrolytes can not only overcome the safety problem caused by the organic electrolytes used in lithium-ion batteries (LIBs) but also show a relatively broad electrochemical stability window (about 3.0 V) compared to the commercial LIB organic electrolytes.[2−5] They also present appealing physical properties, such as a relatively high Li^+ transference number and low viscosity.[6−8] These excellent properties have inspired fundamental research on WIS electrolytes, including the solvation structures, transport properties, etc.[9−22]

Previous studies using small-angle X-ray scattering (SAXS),[16,23−25] small-angle neutron scattering (SANS),[13,26,27] Fourier transform infrared spectroscopy (FTIR) spectroscopy,[11,14,18,19,28] and molecular dynamics (MD) simulations[15,20] have advanced our understanding of the structure and dynamics of the WIS and other electrolytes. Combining SANS and MD simulation, Borodin et al. found a water-rich and anion-rich domain for 21 m lithium bis(trifluoromethane sulfonyl)imide (LiTFSI).[27] The water-rich domain is a percolating channel for fast Li^+ transport with a high lithium-transference number. Using SAXS and MD simulation, our recent work pointed out that two anion solvation structures, the anion solvated structures and the anion networks, coexist in the LiTFSI aqueous solutions.[16] Research works by Zhang et al. and McEldrew et al. also suggested the existence of the anion network in the WIS electrolytes.[11,15]

However, the length scale of solvation structures resolved from SAXS is different from the reported solvation structures at the molecular level,[6,29−32] such as solvent-separated ion pairs (SSIPs), contact ion pairs (CIPs), and aggregate clusters (AGGs). Understanding the relationship between these solvation structures at different length scales is crucial. Moreover, many investigations tried to explain the role of water in WIS electrolytes. Combining femtosecond IR spectroscopy and MD simulations,[18−20,26,33] Lim et al.[18] showed that water had a dual role: bulk-like water forms water channels that play as a medium for lithium-ion transport, whereas interfacial

Received: December 7, 2022
Revised: February 10, 2023
Published: February 23, 2023

https://doi.org/10.1021/acs.chemmater.2c03654
Chem. Mater. 2023, 35, 2088−2094

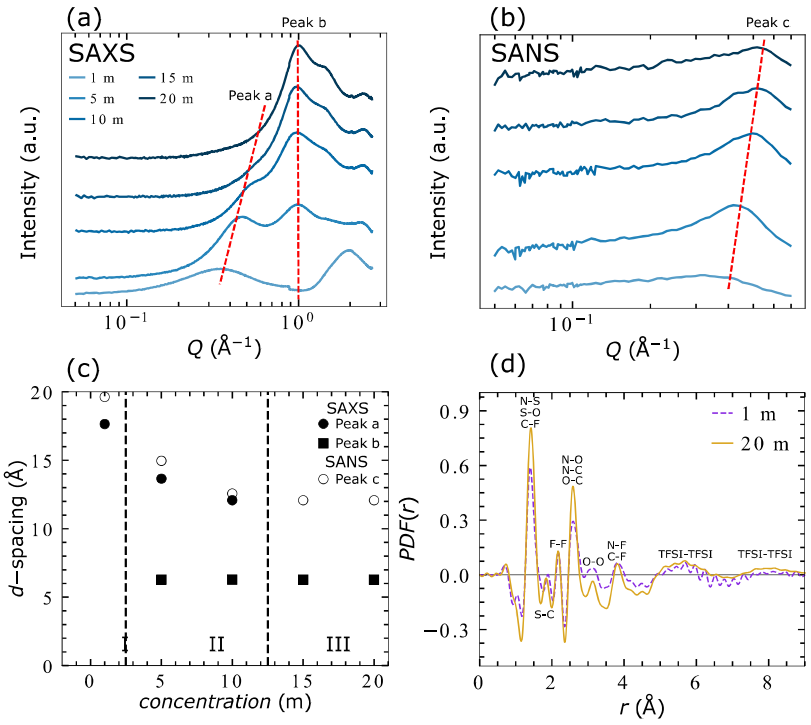

Figure 1. (a) SAXS profiles for LiTFSI/H_2O and (b) SANS profiles for LiTFSI/D_2O at different concentrations. (The data were offset for clarity; Both (a) and (b) shared the same plot legends.) (c) d spacing ($d = 2\pi/q$) as a function of LiTFSI concentrations. (d) Pair distribution functions at 1 and 20 m. (Peaks were identified by their primary contributions from the elements in anions via MD simulations.)

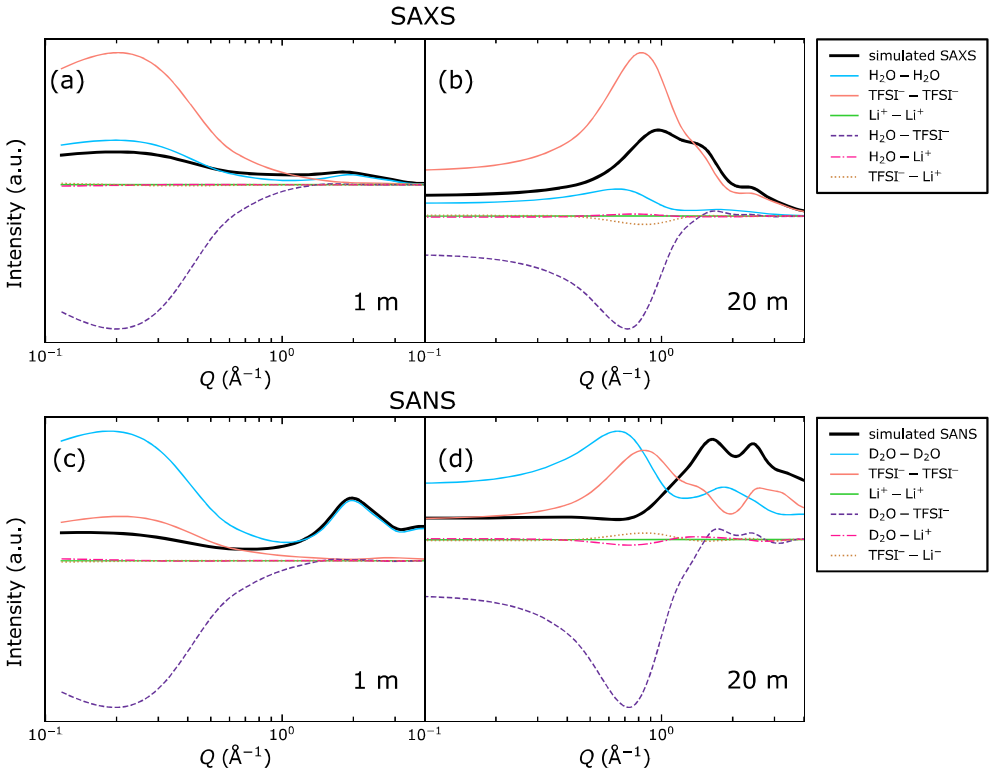

Figure 2. Decomposition of the simulated SAXS and SANS profiles of LiTFSI aqueous solutions. LiTFSI/H_2O (SAXS) at (a) 1 m and (b) 20 m; LiTFSI/D_2O (SANS) at (c) 1 m and (d) 20 m.

water on anion networks act as a lubricant. Our work also supports that the $TFSI^-$ network is formed by bridging water molecules.[16] However, the structural information on water remains elusive.

In this paper, we measured SAXS, SANS, pair distribution function (PDF), and viscosities of LiTFSI aqueous solutions at various concentrations and conducted MD simulations on the same systems. Combining the experiments and MD simulations,

https://doi.org/10.1021/acs.chemmater.2c03654
Chem. Mater. 2023, 35, 2088−2094

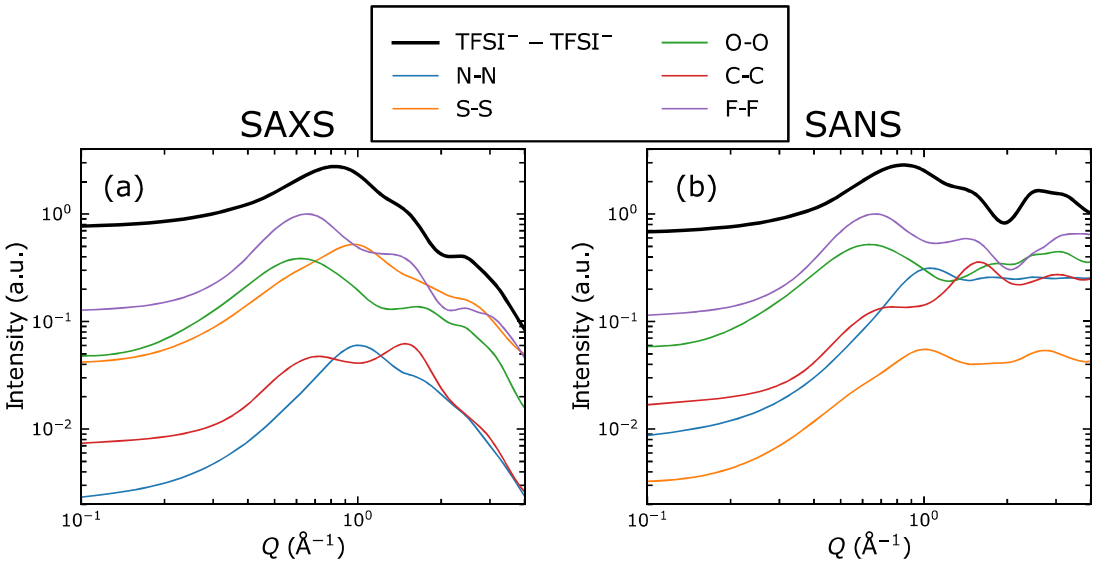

Figure 3. Self-correlations of the elements in the anions for the LiTFSI aqueous solution at 20 m. (a) Simulated SAXS and (b) simulated SANS. The curves are normalized such that F−F correlations have a maximum of unity.

we confirmed that the differences between SAXS and SANS profiles are primarily contributed by the difference in the X-ray and neutron scattering cross sections of the anions. It was found that the $TFSI^-$ solvated structure primarily consists of solvent-separated ion pairs, and the $TFSI^-$ network is mainly composed of contact ion pairs and cation−anion aggregates. In addition, we compared the concentration dependence of the viscosities and the relaxation times associated with the two solvation structures. We found similar trends between the viscosities and the relaxation times associated with the anion network structures composed of the ordering of the anions bridged by the cations (charge alternation) and the solvents (interfacial water). These results suggest that the anion network structure primarily contributes to the transport properties of the WIS electrolytes.

RESULTS AND DISCUSSIONS

LiTFSI in H_2O and D_2O with concentrations of 1, 5, 10, 15, and 20 m were prepared as described in the Methods and Materials. Their SAXS and SANS profiles are shown in Figure 1a,b. In the SAXS profiles, two peaks named Peak a and Peak b can be observed from the dilute to concentrated LiTFSI aqueous solutions, as shown in Figure 1a. Based on our previous results,[16] Peak a and Peak b are ascribed to the TFSI anion solvated structures and the TFSI anion network, respectively. In contrast to SAXS, SANS probes the water molecules more owing to the larger cross-section of deuterons. As shown in Figure 1b, there is only one observable peak named Peak c, whose position shifts to higher q as the concentration increases. Based on the previous studies by Borodin et al.[27] and Horwitz et al.,[26] this peak mainly comes from D_2O−D_2O correlations.

The d spacing of the SAXS and SANS peaks can be calculated using $d = 2\pi/q$, and its relation with the concentrations is shown in Figure 1c. We can see that the d spacing of Peak b remains at around 6.4 Å for all studied concentrations. Peak b is ascribed to the $TFSI^-$ network in which water molecules act as the bridge, keeping the d spacing constant.[16,18] However, the d spacing of Peak a and Peak c gradually decreases from 19.6 to12.0 Å. Peak c could be observed for 15 and 20 m concentrations while Peak a disappears, which indicates that the anion clusters structures are overshadowed by anion network structures while water clusters still exist in between anion networks with the concentration above 15 m. Our SANS data is similar to the literature, as shown in Figure S1.

The SAXS and SANS show the solvation structures of LiTFSI aqueous solutions from long scale length; however, they cannot explain the localized solvation structures. Hence, we compare the partial pair distribution functions of 1 and 20 m LiTFSI aqueous solutions, as shown in Figure 1d. We identified the primary contribution to each peak in the PDFs. It can be observed that the position of most of the peaks remains constant upon concentration increase, which indicates that the intramolecular distances do not change. It is also shown that the transition from intramolecular to intermolecular correlations is at around 5.0 Å.

To thoroughly understand the $S(q)$ evolution, the simulated $S(q)$ was decomposed into contributions between molecular/ionic pairs. Figure 2 shows the simulated SAXS profiles of LiTFSI dissolved in H_2O and SANS profiles of LiTFSI dissolved in D_2O. As already discussed in our previous study, both Peak a and Peak b are mainly contributed by the self-correlation of the anions in SAXS profiles.[34] Peak a is mainly contributed by the peaks from anion−anion and solvent−solvent self-correlations and the "anti-peak" from anion−solvent correlation, implying the existence of the anion−solvent alternation structures at the nanometer length scale. This nanometer-sized structural alternation manifests the anion clusters. On the other hand, Peak b contains two antipeak structures from anion−solvent and anion−cation cross-correlations, indicating that Peak b corresponds to a mixture of anion−solvent and anion−cation alternation at the subnanometer length scale. As for SANS profiles, we found that Peak c consists of anion and solvent self-correlation and the "anti-peak" from anion−solvent cross-correlation, indicating the same structure as Peak a identified in SAXS profiles. Therefore, Peak a and Peak c have similar peak positions (d-spacing). The major difference is that the signal contributed by the anion−anion self-correlation is reduced significantly in the SANS profiles. At high concentration, the "anti-peak" from the anion−solvent correlation compensates their self-correlations, causing the charge alternating feature (Peak b in SAXS profiles) to be implicit in SANS profiles.

https://doi.org/10.1021/acs.chemmater.2c03654
Chem. Mater. 2023, 35, 2088−2094

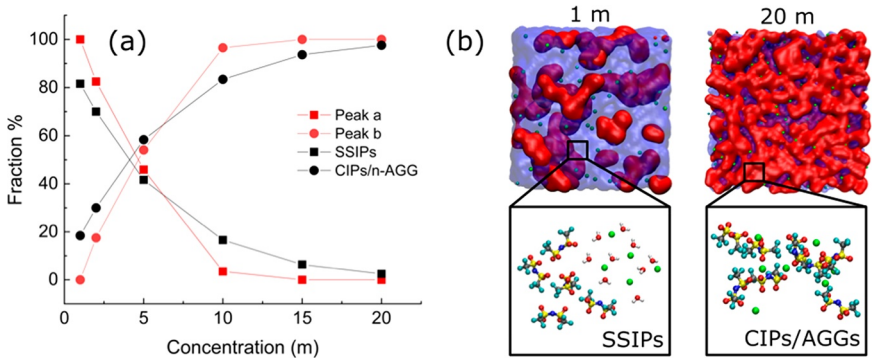

Figure 4. (a) Peak a vs Peak b fraction from SAXS and SSIPs vs CIPs plus AGG fraction from MD simulation. (b) MD simulation snapshots show SSIPs, CIPs, and AGGs.

We further computed the partial SAXS and SANS profiles of each element in anions. Figure 3 shows the self-correlations of N, S, O, C, and F in anions. We found that both S and N self-correlations showed a clear peak at ~1 $Å^{-1}$ in both SAXS and SANS profiles. This feature corresponds to Peak b, which is associated with the ordering of the neighbor anions in anion clusters. We found that Peak b was not observable in SANS primarily due to the relatively small neutron scattering cross-section of the S atoms. Another noticeable feature mentioned in our previous study is that the peak at q = 1−2 $Å^{-1}$ primarily contributes to the correlations of C and F, indicating that the peak corresponds to the correlations between neighboring fluorocarbon chains.

Figure 4 shows the concentration dependence of the fraction of Peak a and b intensities from the SAXS profiles and the fraction of SSIPs and CIPs+AGGs estimated from MD simulations. The similarity between the two plots implies a connection between the structures of anion clusters/networks and the cation coordination around the anions. The decrease in Peak a intensity and the decrease in SSIPs suggest that anion clusters are primarily composed of anions that correspond to SSIPs. This view is consistent with the snapshots shown in Figure 4b, which shows that both nanometer-scale anion clusters and cations are solvated and separated by water domains. The increase in Peak b intensity indicates the enhanced ordering of the alternation between cations and anions. Such ordering is associated with the coordination between Li^+ and the oxygen in $TFSI^-$, which is directly related to CIPs and AGGs, as shown in Figure 4b. However, this relation is qualitative as the SAXS profiles do not provide direct quantitative information about the structures of the aggregates.

The Raman spectra of LiTFSI aqueous solutions with different concentrations under room temperature were also measured, as shown in Figure S2a. We fitted the Raman spectra of LiTFSI aqueous solutions with various concentrations of 700−800 cm^{-1} (S−N stretching mode of the TFSI anion), and the fitting results are shown in Figure S2b−f. Based on the well-accepted approach,[6] the cation−anion clusters could be classified into SSIPs-740 cm^{-1}, CIPs-744−747 cm^{-1}, and AGGs-748 cm^{-1}, respectively. Figure S3 compares the concentration dependence of the fraction of SSIPs and CIPs +AGGs estimated from Raman spectra and MD simulation. We can observe that the fraction with Raman analysis does not agree with the MD results, implying Raman analysis may not provide the quantitative information about the SSIPs, CIPs, and AGGs.

After understanding the solvation structure, we want to investigate how the structure affects the transport properties such as viscosity. According to Maxwell, the viscosity η is directly connected with the shear modulus G_s, which is associated with the strength of the intermolecular interactions, and a single relaxation time of the shear stress τ_s by the equation[35]

$$\eta = G_s\tau_s \quad (1)$$

Figure 5 shows the concentration dependence of the viscosities and average relaxation time τ of Peaks a and b. We also included

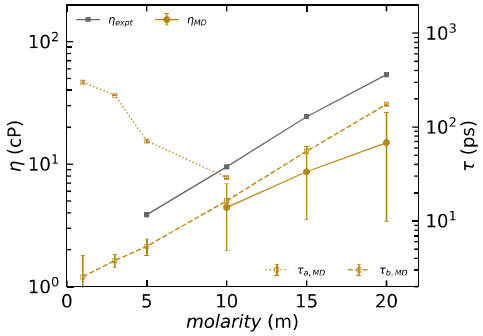

Figure 5. Concentration dependence of the viscosities and the average relaxation time associated with Peaks a and b. The error bars for computed viscosities indicate one standard deviation; the error bars for relaxation times indicate one standard error from fitting. Detailed derivation of one standard error is illustrated in Methods and Materials.

the average relaxation time using 0.9 charge rescaling in Figure S4. We found that the CL&P force field with a 0.8 charge rescaling factor underestimated the viscosity by a factor of 1.7−3.5 in the range of 10−20 m. In comparison, the force field with a 0.9 charge rescaling factor agrees well with the viscosities of the experiments at 10 and 15 m but overestimated the data by a factor of ~1.6 at 20 m. The CL&P force field with a 0.9 charge rescaling seems better at capturing the viscosity of LiTFSI aqueous solutions. What is more important is that the relaxation time of Peak b shows a similar concentration dependence of the viscosities, implying that the relaxation of the anion network mainly dominates the transport property.

CONCLUSION

In summary, we performed SAXS/SANS and viscosity measurements and MD simulations on LiTFSI aqueous electrolytes from 1 to 20 m. The relatively low neutron cross-section from sulfur is the dominant factor that causes SANS to exhibit only one peak. We also found that the ratio of Peak a to Peak b intensity in SAXS files shares a similar trend with the fraction of SSIPs and

https://doi.org/10.1021/acs.chemmater.2c03654
Chem. Mater. 2023, 35, 2088−2094

CIPs/AGGs. The decomposition of SAXS and SANS profiles shows that Peak b is primarily associated with the anion−cation alternation, which is closely related to ion association associated with CIPs and AGGs species. Moreover, we discovered that the concentration dependence of the viscosity is mainly associated with the structural relaxation at the q range of Peak b, corresponding to the cation−anion alternation and the building blocks of ionic networks. This might help us understand the behavior of other transport properties, such as ion conductivity for imide-based electrolytes.

METHODS AND MATERIALS

Sample Preparation. The electrolytes were prepared by dissolving the lithium bis(trifluoromethane sulfonyl)imide (LiTFSI, >99%, Sigma-Aldrich) in high purity water, which has a conductivity of 18.2 MΩ × cm at 25 °C, and deuterium oxide (Sigma-Aldrich). All the salts and solvents are used without further purification. All the electrolytes were prepared by molality (mole-salt in kg-solvent) described as abbreviated concentrations (1, 5, 10, 15, and 20 m).

Small-Angle X-ray Scattering. SAXS experiments were measured at the 12 ID-B and C of the Advanced Photon Source (APS) station of Argonne National Laboratory. The scattering vector, q, was calibrated using silver behenate. The samples were loaded into 2 mm diameter quartz capillary tubes and sealed with epoxy for the SAXS measurement.

Small-Angle Neutron Scattering. The SANS data were acquired at the GP-SANS (CG2), High Flux Isotope Reactor, Oak Ridge National Laboratory (ORNL).[36,37] The instrument was configured with sample-to-detector distances of 7 m and 1 m combined with the wavelength of 4.75 Å, covering a momentum space of 0.05 $Å^{-1} < Q < 0.7\ Å^{-1}$. Absolute scale intensities were calibrated with a porous silica standard sample. Data reduction, including detector sensitivity and background corrections, was performed following standard procedures.[38,39] The different LiTFSI aqueous solution samples were placed in quartz cuvettes of 1 mm path length from Hellma (Plainview, NY, U.S.A.).

Pair Distribution Function. Pair distribution function data were collected at 28-ID-1 in the National Synchrotron Light Source II (NSLS-II) at Brookhaven National Laboratory. The 2D diffraction data were collected with a PerkinElmer amorphous silicon detector, integrated into 1D diffraction patterns with DIOPTAS[40] and Fourier transformed into real-space pair distribution functions with xPDF suite.

Raman Spectroscopy. Raman spectra of the samples were collected at the GSECARS (APS, Argonne, U.S.A.) under room temperature. The Raman system had an excitation wavelength of 532 nm.

MD Simulation. The bonded and nonbonded parameters for the anion were taken from CL&P force field, which is an interatomic potential optimized for ionic liquids.[41] The OPLS-AA parameters[34] and SPC/E water model were used.[42] For the simulated SAXS and SANS profiles and the calculation of SSIPs, CIPs, and AGGs, the partial charges of the anions and cations are rescaled by a factor of 0.8, which is the rescaling factor we used in our previous study for the structures of the imide-based Li salt aqueous electrolytes. However, it was shown that the viscosity was underestimated by a factor of 1.6 if a 0.8 charge rescaling was used but was overestimated by a factor of 2.6 if no charge rescaling was used.[43,44] Therefore, besides a 0.8 charge rescaling, we added additional calculations of the viscosities with 0.9 charge rescaling. Large-scale Atomic/Molecular Massively Parallel Simulator (LAMMPS) was used in this study.[45] Packmol[38] randomly initialized 4495 water molecules and 81 LiTFSI/mol, and the topology of the molecules was prepared by Moltemplate.[46] We first maintained the temperature at 400 K for 200 ps and quenched it to 300 K within 100 ps. Next, we ran an isothermal−isobaric (NPT) ensemble for at least 2 ns to obtain the equilibrated density. Finally, we obtained 40 ns of trajectories produced. We set the time step to 2 fs, and the Nosé−Hoover thermostat was used. VMD[40] visualized the snapshots.

Data Analysis for MD Simulations. The simulated SAXS and SANS profiles were computed using LiquidLib.[47] For ion associations, we counted the number of coordinated anions around the cations in each snapshot and categorized the coordination numbers into SSIPs (0 anion), CIPs (1 anion), and AGGs (>2 anions). The simulated viscosities are computed via integrating the stress autocorrelation function, also known as the Green−Kubo relation:

$$\eta_{MD} = \frac{V}{3k_bT}\int_0^\infty \sum_{i<j} \frac{\langle \sigma_{ij}(t_0)\sigma_{ij}(t_0+t)\rangle}{\langle \sigma_{ij}(t_0)^2\rangle}\,\mathrm{d}t$$

where $i, j \in x, y, z$

where V is the volume of the simulation box, k_b is the Boltzmann constant, T is the temperature, and σ_{ij} are the off-diagonal entries of the stress tensor. To compute the relaxation times of Peak a and Peak b, we first computed the coherent intermediate scattering functions, $F(q, t)$, which is the temporal Fourier transform of the coherent dynamic structure factor, $S(q, E)$, directly measured by coherent inelastic neutron scattering experiments. The simulated $F(q, t)$ were then fitted by stretched exponential functions:

$$F(q, t) = f e^{-\left(\frac{t}{\tau}\right)^{\beta}}$$

where f is the prefactor, τ is the relaxation time, and β is the stretch exponent. Note that f, τ, and β are fitting parameters and are functions of q. The average relaxation times for Peak a and Peak b were then computed via

$$\tau_i(q = q_i) = \frac{\tau}{\beta}\Gamma\left(\frac{1}{\beta}\right) \quad \text{where } i = a \text{ or } b$$

The q_i value indicates the peak position, and Γ represents the Gamma function. The $F(q, t)$ values were calculated with LiquidLib. The one standard error of τ_i was computed via the following equation:

$$\sigma_i = \sqrt{\sigma_\tau^2\left(\frac{\partial \tau_i}{\partial \tau}\right)^2 + \sigma_\beta^2\left(\frac{\partial \tau_i}{\partial \beta}\right)^2}$$

where σ_τ and σ_β are one standard errors of τ and β, which were derived from the square root of the main diagonal terms of the covariance matrix of the parameters from fitting.

ASSOCIATED CONTENT

Supporting Information

The Supporting Information is available free of charge at https://pubs.acs.org/doi/10.1021/acs.chemmater.2c03654.

Comparisons of the SANS peak positions identified in this study and Horwitz et al.;[26] Raman spectra of LiTFSI aqueous solutions with different concentrations between 660 and 820 cm^{-1}, fitting curves of Raman spectra for 1 m, 5 m, 10 m, 15 m, and 20 m LiTFSI aqueous solutions; SSIPs vs CIPs plus AGG fraction from Raman spectra and MD simulations; concentration dependence of the viscosities and the average relaxation time associated with Peaks a and b, and results computed by MD simulations including both 0.8 and 0.9 charge rescaling (PDF)

AUTHOR INFORMATION

Corresponding Authors

Y Z − *Department of Nuclear, Plasma, and Radiological Engineering, Beckman Institute for Advanced Science and Technology, and Department of Electrical and Computer Engineering, University of Illinois at Urbana−Champaign, Urbana, Illinois 61801, United States; Joint Center for Energy Storage Research, Argonne National Laboratory, Lemont,*

https://doi.org/10.1021/acs.chemmater.2c03654
Chem. Mater. 2023, 35, 2088−2094

Illinois 60439, United States; Department of Nuclear Engineering and Radiological Sciences, University of Michigan, Ann Arbor, Michigan 48109, United States; orcid.org/0000-0002-7339-8342; Email: zhyang@illinois.edu

Tao Li − *Department of Chemistry and Biochemistry, Northern Illinois University, DeKalb, Illinois 60115, United States; X-ray Science Division and Joint Center for Energy Storage Research, Argonne National Laboratory, Lemont, Illinois 60439, United States;* orcid.org/0000-0002-4913-4486; Email: tli4@niu.edu

Authors

Xinyi Liu − *Department of Chemistry and Biochemistry, Northern Illinois University, DeKalb, Illinois 60115, United States;* orcid.org/0000-0001-6092-2558

Shao-Chun Lee − *Department of Nuclear, Plasma, and Radiological Engineering and Beckman Institute for Advanced Science and Technology, University of Illinois at Urbana−Champaign, Urbana, Illinois 61801, United States;* orcid.org/0000-0002-0665-5337

Soenke Seifert − *X-ray Science Division, Argonne National Laboratory, Lemont, Illinois 60439, United States*

Lilin He − *Neutron Scattering Division, Oak Ridge National Laboratory, Oak Ridge, Tennessee 37831-6393, United States*

Changwoo Do − *Neutron Scattering Division, Oak Ridge National Laboratory, Oak Ridge, Tennessee 37831-6393, United States;* orcid.org/0000-0001-8358-8417

Randall E. Winans − *X-ray Science Division and Joint Center for Energy Storage Research, Argonne National Laboratory, Lemont, Illinois 60439, United States;* orcid.org/0000-0002-7080-7673

Gihan Kwon − *National Synchrotron Light Source II, Brookhaven National Laboratory, Upton, New York 11973, United States;* orcid.org/0000-0002-7963-2136

Complete contact information is available at: https://pubs.acs.org/10.1021/acs.chemmater.2c03654

Author Contributions

#These authors contributed equally: Xinyi Liu and Shao-Chun Lee.

Notes

The authors declare no competing financial interest.

■ ACKNOWLEDGMENTS

This work was supported as part of the Joint Center for Energy Storage Research, an Energy Innovation Hub funded by the U.S. Department of Energy, Office of Science, Basic Energy Sciences. T. Li is thankful for the support by the U.S. National Science Foundation (Grant No. 2120559). A portion of this research used resources at the Spallation Neutron Source, a DOE Office of Science User Facility operated by the Oak Ridge National Laboratory. This research used resources of the Advanced Photon Source, a U.S. Department of Energy (DOE) Office of Science User Facility operated for the DOE Office of Science by Argonne National Laboratory under Contract No. AC02-06CH11357. This research used the 28-ID-1 (PDF) beamline of the National Synchrotron Light Source II, a U.S. Department of Energy (DOE) Office of Science User Facility operated for the DOE Office of Science by Brookhaven National Laboratory under Contract No. DE-SC0012704.

■ REFERENCES

(1) Suo, L.; Borodin, O.; Gao, T.; Olguin, M.; Ho, J.; Fan, X.; Luo, C.; Wang, C.; Xu, K. "Water-in-salt" electrolyte enables high-voltage aqueous lithium-ion chemistries. *Science* **2015**, *350* (6263), 938−943.

(2) Yamada, Y.; Usui, K.; Sodeyama, K.; Ko, S.; Tateyama, Y.; Yamada, A. Hydrate-melt electrolytes for high-energy-density aqueous batteries. *Nature Energy* **2016**, *1* (10), 16129.

(3) Xu, J.; Ji, X.; Zhang, J.; Yang, C.; Wang, P.; Liu, S.; Ludwig, K.; Chen, F.; Kofinas, P.; Wang, C. Aqueous electrolyte design for super-stable 2.5 V LiMn2O4 ‖ Li4Ti5O12 pouch cells. *Nature Energy* **2022**, *7*, 186−193.

(4) Wang, Y.; Yi, J.; Xia, Y. Recent Progress in Aqueous Lithium-Ion Batteries. *Adv. Energy Mater.* **2012**, *2* (7), 830−840.

(5) Liu, S.; Ye, S. H.; Li, C. Z.; Pan, G. L.; Gao, X. P. Rechargeable Aqueous Lithium-Ion Battery of TiO2/LiMn2O4 with a High Voltage. *J. Electrochem. Soc.* **2011**, *158* (12), A1490−1497.

(6) Suo, L.; Oh, D.; Lin, Y.; Zhuo, Z.; Borodin, O.; Gao, T.; Wang, F.; Kushima, A.; Wang, Z.; Kim, H. C.; Qi, Y.; Yang, W.; Pan, F.; Li, J.; Xu, K.; Wang, C. How Solid-Electrolyte Interphase Forms in Aqueous Electrolytes. *J. Am. Chem. Soc.* **2017**, *139* (51), 18670−18680.

(7) Suo, L.; Han, F.; Fan, X.; Liu, H.; Xu, K.; Wang, C. Water-in-Salt" electrolytes enable green and safe Li-ion batteries for large scale electric energy storage applications. *Journal of Materials Chemistry A* **2016**, *4* (17), 6639−6644.

(8) Tan, J.; Liu, J. Electrolyte Engineering Toward High-Voltage Aqueous Energy Storage Devices. *Energy & Environmental Materials* **2021**, *4* (3), 302−306.

(9) Zheng, J.; Lochala, J. A.; Kwok, A.; Deng, Z. D.; Xiao, J. Research Progress towards Understanding the Unique Interfaces between Concentrated Electrolytes and Electrodes for Energy Storage Applications. *Adv. Sci. (Weinh)* **2017**, *4* (8), 1700032.

(10) Zhang, Y.; Maginn, E. J. Water-In-Salt LiTFSI Aqueous Electrolytes (2): Transport Properties and Li(+) Dynamics Based on Molecular Dynamics Simulations. *J. Phys. Chem. B* **2021**, *125* (48), 13246−13254.

(11) Zhang, Y.; Lewis, N. H. C.; Mars, J.; Wan, G.; Weadock, N. J.; Takacs, C. J.; Lukatskaya, M. R.; Steinruck, H. G.; Toney, M. F.; Tokmakoff, A.; Maginn, E. J. Water-in-Salt LiTFSI Aqueous Electrolytes. 1. Liquid Structure from Combined Molecular Dynamics Simulation and Experimental Studies. *J. Phys. Chem. B* **2021**, *125* (17), 4501−4513.

(12) Yu, Z.; Balsara, N. P.; Borodin, O.; Gewirth, A. A.; Hahn, N. T.; Maginn, E. J.; Persson, K. A.; Srinivasan, V.; Toney, M. F.; Xu, K.; Zavadil, K. R.; Curtiss, L. A.; Cheng, L. Beyond Local Solvation Structure: Nanometric Aggregates in Battery Electrolytes and Their Effect on Electrolyte Properties. *ACS Energy Letters* **2022**, *7* (1), 461−470.

(13) Tan, P.; Yue, J.; Yu, Y.; Liu, B.; Liu, T.; Zheng, L.; He, L.; Zhang, X.; Suo, L.; Hong, L. Solid-Like Nano-Anion Cluster Constructs a Free Lithium-Ion-Conducting Superfluid Framework in a Water-in-Salt Electrolyte. *J. Phys. Chem. C* **2021**, *125* (22), 11838−11847.

(14) Popov, I.; Sacci, R. L.; Sanders, N. C.; Matsumoto, R. A.; Thompson, M. W.; Osti, N. C.; Kobayashi, T.; Tyagi, M.; Mamontov, E.; Pruski, M.; Cummings, P. T.; Sokolov, A. P. Critical Role of Anion−Solvent Interactions for Dynamics of Solvent-in-Salt Solutions. *J. Phys. Chem. C* **2020**, *124* (16), 8457−8466.

(15) McEldrew, M.; Goodwin, Z. A. H.; Bi, S.; Kornyshev, A. A.; Bazant, M. Z. Ion Clusters and Networks in Water-in-Salt Electrolytes. *J. Electrochem. Soc.* **2021**, *168* (5), No. 050514.

(16) Liu, X.; Yu, Z.; Sarnello, E.; Qian, K.; Seifert, S.; Winans, R. E.; Cheng, L.; Li, T. Microscopic Understanding of the Ionic Networks of "Water-in-Salt" Electrolytes. *Energy Material Advances* **2021**, *2021*, 7368420.

(17) Liu, X.; Lee, S.-C.; Seifer, S.; Winans, R. E.; Cheng, L.; Z, Y.; Li, T. Insight into the nanostructure of "water in salt" solutions: A SAXS/WAXS study on imide-based lithium salts aqueous solutions. *Energy Storage Materials* **2022**, *45*, 696−703.

(18) Lim, J.; Park, K.; Lee, H.; Kim, J.; Kwak, K.; Cho, M. Nanometric Water Channels in Water-in-Salt Lithium Ion Battery Electrolyte. *J. Am. Chem. Soc.* **2018**, *140* (46), 15661−15667.
(19) Kim, J.; Koo, B.; Lim, J.; Jeon, J.; Lim, C.; Lee, H.; Kwak, K.; Cho, M. Dynamic Water Promotes Lithium-Ion Transport in Superconcentrated and Eutectic Aqueous Electrolytes. *ACS Energy Letters* **2022**, *7*, 189−196.
(20) Jeon, J.; Lee, H.; Choi, J.-H.; Cho, M. Modeling and Simulation of Concentrated Aqueous Solutions of LiTFSI for Battery Applications. *J. Phys. Chem. C* **2020**, *124* (22), 11790−11799.
(21) Ding, M. S.; von Cresce, A.; Xu, K. Conductivity, Viscosity, and Their Correlation of a Super-Concentrated Aqueous Electrolyte. *J. Phys. Chem. C* **2017**, *121* (4), 2149−2153.
(22) Galle Kankanamge, S. R.; Kuroda, D. G. Molecular Structure, Chemical Exchange, and Conductivity Mechanism of High Concentration LiTFSI Electrolytes. *J. Phys. Chem. B* **2020**, *124* (10), 1965−1977.
(23) Qian, K.; Winans, R. E.; Li, T. Insights into the Nanostructure, Solvation, and Dynamics of Liquid Electrolytes through Small-Angle X-Ray Scattering. *Adv. Energy Mater.* **2021**, *11* (4), 2002821.
(24) Qian, K.; Yu, Z.; Liu, Y.; Gosztola, D. J.; Winans, R. E.; Cheng, L.; Li, T. Understanding fluorine-free electrolytes via small-angle X-ray scattering. *Journal of Energy Chemistry* **2022**, *70*, 340−346.
(25) Qian, K.; Seifert, S.; Winans, R. E.; Li, T. Understanding Solvation Behavior of the Saturated Electrolytes with Small/Wide-Angle X-ray Scattering and Raman Spectroscopy. *Energy Fuels* **2021**, *35* (23), 19849−19855.
(26) Horwitz, G.; Hark, E.; Steinberg, P. Y.; Cavalcanti, L. P.; Risse, S.; Corti, H. R. The Nanostructure of Water-in-Salt Electrolytes Revisited: Effect of the Anion Size. *ACS Nano* **2021**, *15*, 11564−11572.
(27) Borodin, O.; Suo, L.; Gobet, M.; Ren, X.; Wang, F.; Faraone, A.; Peng, J.; Olguin, M.; Schroeder, M.; Ding, M. S.; Gobrogge, E.; von Wald Cresce, A.; Munoz, S.; Dura, J. A.; Greenbaum, S.; Wang, C.; Xu, K. Liquid Structure with Nano-Heterogeneity Promotes Cationic Transport in Concentrated Electrolytes. *ACS Nano* **2017**, *11* (10), 10462−10471.
(28) Zhang, M.; Hao, H.; Zhou, D.; Duan, Y.; Wang, Y.; Bian, H. Understanding the Microscopic Structure of a "Water-in-Salt" Lithium Ion Battery Electrolyte Probed with Ultrafast IR Spectroscopy. *J. Phys. Chem. C* **2020**, *124* (16), 8594−8604.
(29) Wang, J.; Yamada, Y.; Sodeyama, K.; Chiang, C. H.; Tateyama, Y.; Yamada, A. Superconcentrated electrolytes for a high-voltage lithium-ion battery. *Nat. Commun.* **2016**, *7*, 12032.
(30) Yamada, Y.; Furukawa, K.; Sodeyama, K.; Kikuchi, K.; Yaegashi, M.; Tateyama, Y.; Yamada, A. Unusual stability of acetonitrile-based superconcentrated electrolytes for fast-charging lithium-ion batteries. *J. Am. Chem. Soc.* **2014**, *136* (13), 5039−5046.
(31) Chang, Z.; Qiao, Y.; Yang, H.; Deng, H.; Zhu, X.; He, P.; Zhou, H. Beyond the concentrated electrolyte: further depleting solvent molecules within a Li+ solvation sheath to stabilize high-energy-density lithium metal batteries. *Energy Environ. Sci.* **2020**, *13* (11), 4122−4131.
(32) Su, L.; Zhao, X.; Yi, M.; Charalambous, H.; Celio, H.; Liu, Y.; Manthiram, A. Uncovering the Solvation Structure of $LiPF_6$-Based Localized Saturated Electrolytes and Their Effect on $LiNiO_2$-Based Lithium-Metal Batteries. *Adv. Energy Mater.* **2022**, *12* (36), 2201911.
(33) Gonzalez, M. A.; Borodin, O.; Kofu, M.; Shibata, K.; Yamada, T.; Yamamuro, O.; Xu, K.; Price, D. L.; Saboungi, M. L. Nanoscale Relaxation in "Water-in-Salt" and "Water-in-Bisalt" Electrolytes. *J. Phys. Chem. Lett.* **2020**, *11* (17), 7279−7284.
(34) Sharma, S.; Ivanov, A. S.; Margulis, C. J. A Brief Guide to the Structure of High-Temperature Molten Salts and Key Aspects Making Them Different from Their Low-Temperature Relatives, the Ionic Liquids. *J. Phys. Chem. B* **2021**, *125* (24), 6359−6372.
(35) Rötger, H. Relaxation times and viscosity. *J. Non-Cryst. Solids* **1974**, *14* (1), 201−217.
(36) Heller, W. T.; Cuneo, M.; Debeer-Schmitt, L.; Do, C.; He, L.; Heroux, L.; Littrell, K.; Pingali, S. V.; Qian, S.; Stanley, C.; Urban, V. S.; Wu, B.; Bras, W. The suite of small-angle neutron scattering instruments at Oak Ridge National Laboratory. *J. Appl. Crystallogr.* **2018**, *51* (2), 242−248.
(37) Zhao, J. K.; Gao, C. Y.; Liu, D. The extendedQ-range small-angle neutron scattering diffractometer at the SNS. *J. Appl. Crystallogr.* **2010**, *43* (5), 1068−1077.
(38) Arnold, O.; Borreguero, J. M.; Buts, A.; Campbell, S. I.; Chapon, L.; Doucet, M.; Draper, N.; Ferraz Leal, R.; Gigg, M. A.; Lynch, V. E.; Markvardsen, A.; Mikkelson, D. J.; Mikkelson, R. L.; Miller, R.; Palmen, K.; Parker, P.; Passos, G.; Perring, T. G.; Peterson, P. F.; Ren, S.; Reuter, M. A.; Savici, A. T.; Taylor, J. W.; Taylor, R. J.; Tolchenov, R.; Zhou, W.; Zikovsky, J.; Bilheux, J. C. Mantid-Data analysis and visualization package for neutron scattering and mu SR experiments. *Nuclear Instruments and Methods in Physics Research Section A: Accelerators, Spectrometers, Detectors and Associated Equipment* **2014**, *764*, 156−166.
(39) Heller, W. T.; Hetrick, J.; Bilheux, J.; Calvo, J. M. B.; Chen, W.-R.; DeBeer-Schmitt, L.; Do, C.; Doucet, M.; Fitzsimmons, M. R.; Godoy, W. F.; Granroth, G. E.; Hahn, S.; He, L.; Islam, F.; Lin, J.; Littrell, K. C.; McDonnell, M.; McGaha, J.; Peterson, P. F.; Pingali, S. V.; Qian, S.; Savici, A. T.; Shang, Y.; Stanley, C. B.; Urban, V. S.; Whitfield, R. E.; Zhang, C.; Zhou, W.; Billings, J. J.; Cuneo, M. J.; Leal, R. M. F.; Wang, T.; Wu, B. drtsans: The data reduction toolkit for small-angle neutron scattering at Oak Ridge National Laboratory. *SoftwareX* **2022**, *19*, 101101.
(40) Prescher, C.; Prakapenka, V. B. DIOPTAS: a program for reduction of two-dimensional X-ray diffraction data and data exploration. *High Pressure Research* **2015**, *35* (3), 223−230.
(41) Canongia Lopes, J. N.; Pádua, A. A. H. CL&P: A generic and systematic force field for ionic liquids modeling. *Theor. Chem. Acc.* **2012**, *131* (3), 1129.
(42) Berendsen, H. J. C.; Grigera, J. R.; Straatsma, T. P. The missing term in effective pair potentials. *J. Phys. Chem.* **1987**, *91* (24), 6269−6271.
(43) Li, Z.; Bouchal, R.; Mendez-Morales, T.; Rollet, A. L.; Rizzi, C.; Le Vot, S.; Favier, F.; Rotenberg, B.; Borodin, O.; Fontaine, O.; Salanne, M. Transport Properties of Li-TFSI Water-in-Salt Electrolytes. *J. Phys. Chem. B* **2019**, *123* (49), 10514−10521.
(44) Li, Z.; Robertson, L. A.; Shkrob, I. A.; Smith, K. C.; Cheng, L.; Zhang, L.; Moore, J. S.; Z, Y. Realistic Ion Dynamics through Charge Renormalization in Nonaqueous Electrolytes. *J. Phys. Chem. B* **2020**, *124* (15), 3214−3220.
(45) Plimpton, S. Fast Parallel Algorithms for Short-Range Molecular Dynamics. *J. Comput. Phys.* **1995**, *117* (1), 1−19.
(46) Jewett, A. I.; Stelter, D.; Lambert, J.; Saladi, S. M.; Roscioni, O. M.; Ricci, M.; Autin, L.; Maritan, M.; Bashusqeh, S. M.; Keyes, T.; Dame, R. T.; Shea, J.-E.; Jensen, G. J.; Goodsell, D. S. Moltemplate: A Tool for Coarse-Grained Modeling of Complex Biological Matter and Soft Condensed Matter Physics. *J. Mol. Biol.* **2021**, *433* (11), 166841.
(47) Walter, N. P.; Jaiswal, A.; Cai, Z.; Zhang, Y. LiquidLib: A comprehensive toolbox for analyzing classical and ab initio molecular dynamics simulations of liquids and liquid-like matter with applications to neutron scattering experiments. *Comput. Phys. Commun.* **2018**, *228*, 209−218.

https://doi.org/10.1021/acs.chemmater.2c03654
Chem. Mater. 2023, 35, 2088−2094